Inorganica Chimica Acta 362 (2009) 4191–4197

Contents lists available at ScienceDirect

Inorganica Chimica Acta

journal homepage: www.elsevier.com/locate/ica

Chemistry of molecular and supramolecular structures of vanadium(IV) and dioxygen-bridged V(V) complexes incorporating tridentate hydrazone ligands

Neema Ani Mangalam [a], Sarika Sivakumar [a], S.R. Sheeja [a], M.R. Prathapachandra Kurup [a,*], Edward R.T. Tiekink [b]

[a] Department of Applied Chemistry, Cochin University of Science and Technology, Kochi, Kerala 682 022, India
[b] Department of Chemistry, University of Texas, San Antonio, TX 78249, USA

ARTICLE INFO

Article history:
Received 23 March 2009
Received in revised form 9 June 2009
Accepted 16 June 2009
Available online 23 June 2009

Keywords:
Crystal structure
Hydrazones
Vanadium(IV/V) complexes
EPR spectra
Binuclear complexes
Supramolecular structures

ABSTRACT

Four hydrazone ligands: 2-benzoylpyridine benzoyl hydrazone (HBPB), di-2-pyridyl ketone nicotinoyl hydrazone (HDKN), quinoline-2-carbaldehyde benzoyl hydrazone (HQCB), and quinoline-2-carbaldehyde nicotinoyl hydrazone (HQCN) and four of their complexes with vanadyl salts have been synthesized and characterized. Single crystals of HBPB and complexes $[VO(BPB)(\mu_2\text{-}O)]_2$ (**1**) and $[VO(DKN)(\mu_2\text{-}O)]_2{\cdot}\frac{1}{2}H_2O$ (**2**) were isolated and characterized by X-ray crystallography. Each of the complexes exhibits a binuclear structure where two vanadium(V) atoms are bridged by two oxygen atoms to form distorted octahedral structures within *cis*-N_2O_4 donor sets. In most complexes, the uninegative anions function as tridentate ligands, coordinating through the pyridyl- and azomethine-nitrogen atoms and enolic oxygen whereas in complex $[VO(HQCN)(SO_4)]SO_4{\cdot}4H_2O$ (**4**) the ligand is coordinated in the keto form. Complexes $[VO(QCB)(OMe)]{\cdot}1.5H_2O$ (**3**) and **4** are found to be EPR active and showed well-resolved axial anisotropy with two sets of eight line pattern.

1. Introduction

Interest in coordination chemistry of aroylhydrazones has been a subject of enthusiastic research since they show a wide range of catalytic properties, especially those examples derived from heterocyclic aldehydes or ketones [1]. The heightened interest in vanadium coordination complexes stems from its importance in biological systems, which is only now beginning to be fully appreciated [2]. Vanadium may or may not play an essential role in normal mammalian metabolism [2]. However, at pharmacological concentrations, some species are potential therapeutic agents [3,4]. Thus, the insulin-enhancing, insulin mimetic properties of oxovanadium(V) complexes, their use as model complexes for the active site of vanadoenzymes, and their use as catalysts in biological and industrial processes have been reported [5–9]. Furthermore, these compounds exhibit potential as anti-tumour agents by inhibiting growth of malignant cell lines by induction of cell-cycle arrest and/or cytotoxic effects [10]. Although most known insulin-like complexes contain vanadium in oxidation state +IV, vanadium(V) compounds have also been found to have insulin-like properties [11]. Depending on the number and type of donor atoms, and the nature of substitution in these oligodentate ligands, a variety of mononuclear and polynuclear oxo-, dioxo-vanadium(V) complexes and complex clusters have been reported [12–14]. The metal centres in oxovanadium(V) monomers with a N_2O_3 chromophore usually exhibit square pyramidal or trigonal bipyramidal geometries. The two five coordinate vanadium(V) centres often dimerise into octahedral bis(μ-oxo)-bridged complexes *via* (L)V=O–V=O(L) intermolecular interactions with highly asymmetric metal-(μ-O) distances.

In view of importance of vanadium complexes, we present here the synthesis, spectroscopic characterization of VO^{2+} and VO_2^+ complexes of some aroyl hydrazones and crystal structure determinations of two representative binuclear (μ_2-oxo)-bridged vanadium species.

2. Experimental

2.1. Materials

Di-2-pyridylketone (Aldrich), 2-benzoylpyridine (Aldrich), quinoline-2-carbaldehyde (Aldrich), Benzhydrazide (Aldrich), and nicotinic hydrazide (Aldrich), vanadyl sulfate (Aldrich) and $VO(acac)_2$ (E-Merck) were used as received. Solvents were purified by standard procedures before use.

2.2. Syntheses of ligands

All the hydrazone ligands were synthesized by adapting the earlier reported procedure, namely via condensation between

* Corresponding author. Tel.: +91 484 2575804; fax: +91 484 2577595.
E-mail address: mrp@cusat.ac.in (M.R. Prathapachandra Kurup).

0020-1693/$ - see front matter © 2009 Elsevier B.V. All rights reserved.
doi:10.1016/j.ica.2009.06.029

appropriate aldehyde/ketone with the respective acid hydrazide as described below [15]. The chemical structures and abbreviations for the ligands are given in Fig. 1.

2.2.1. Synthesis of 2-benzoylpyridine benzoyl hydrazone (HBPB)

A methanol solution of benzoic hydrazide (0.136 g, 1 mmol) was refluxed with 2-benzoylpyridine (0.183 g, 1 mmol) continuously for 4 h after adding a few drops of glacial acetic acid. There was no immediate formation of the product. Then the reaction mixture was kept aside for slow evaporation at room temperature. After 3–4 days, colourless block-shaped crystals suitable for single crystal analyses were formed which were carefully separated (Scheme 1). Yield: 79%, m.p.: 128–130 °C. Elemental *Anal.* Calc.: C, 75.73; H, 5.02; N, 13.94. Found: C, 75.46; H, 5.23; N, 13.98%.

Selected IR (cm^{-1}) bands: ν(N–H) 3063; ν(C=O) 1678; ν(C=N) 1571.

Electronic absorption bands (MeCN) λ_{max} (nm): 233, 271, 322.

2.2.2. Synthesis of di-2-pyridyl ketone nicotinoyl hydrazone hemihydrate (HDKN·0.5H$_2$O)

Colourless HDKN·0.5H_2O was synthesized from di-2-pyridyl ketone and nicotinoyl hydrazide by a procedure similar to that described for HBPB. Yield: 84%, m.p.: 158–160 °C. Elemental *Anal.* Calc. for HDKN·0.5H_2O: C, 65.37; H, 4.52; N, 22.42. Found: C, 65.94; H, 4.26; N, 22.47%.

Selected IR (cm^{-1}) bands: ν(N–H) 2928; ν(C=O) 1689; ν(C=N) 1579.

Electronic absorption bands (MeCN) λ_{max} (nm): 223, 269, 318.

2.2.3. Synthesis of quinoline-2-carbaldehyde benzoyl hydrazone sesquihydrate (HQCB·1.5H$_2$O)

Pale-yellow HQCB·1.5H_2O was synthesized from quinoline-2-carbaldehyde and benzoic hydrazide. Yield: 89%, m.p.: 143–145 °C. Elemental *Anal.* Calc. for HQCB·1.5H_2O: C, 67.54; H, 5.33; N, 13.90. Found: C, 67.81; H, 4.86; N, 14.40%.

Selected IR (cm^{-1}) bands: ν(N–H) 3191; ν(C=O) 1655; ν(C=N) 1593.

Electronic absorption bands (MeCN) λ_{max} (nm): 240, 277, 326.

2.2.4. Synthesis of quinoline-2-carbaldehyde nicotinoyl hydrazone sesquihydrate (HQCN·1.5H$_2$O)

Colourless HQCN·1.5H_2O was prepared in the same way as for HDKN except quinoline-2-carbaldehyde was used instead of di-2-pyridyl ketone. Yield: 84%, m.p.: 140–142 °C. Elemental *Anal.* Calc. for HQCN·1.5H_2O: C, 63.36; H, 4.98; N, 18.47. Found: C, 63.16; H, 4.59; N, 18.58%.

Selected IR (cm^{-1}) bands: ν(N–H) 3173; ν(C=O) 1656; ν(C=N) 1591.

Electronic absorption bands (MeCN) λ_{max} (nm): 241, 279, 315.

2.3. Syntheses of complexes

*2.3.1. Syntheses of [VO(BPB)(μ_2-O)]$_2$ (**1**)*

Complex **1** was prepared by refluxing a methanolic solution of HBPB (1 mmol, 0.301 g) and vanadyl sulfate (1 mmol, 0.163 g) for 5 h. The resulting solution was allowed to stand at room temperature and after slow evaporation, yellow crystals of complex **1** were separated, filtered and washed with ether and dried over P_4O_{10} *in vacuo*.

[VO(BPB)(μ_2-O)]$_2$: Yield: 63%, m.p.: 225–227 °C. λ_m (DMF): 6 $ohm^{-1}\,cm^2\,mol^{-1}$. Elemental *Anal.* Calc.: C, 60.01; H, 3.87; N, 10.77. Found: C, 59.86; H, 4.28; N, 11.31%.

*2.3.2. Synthesis of [VO(DKN)(μ_2-O)]$_2$·2H$_2$O (**2**)*

To a solution of HDKN (1 mmol, 0.312 g) in methanol, a DMF–methanol mixture of VO(acac)$_2$ (1 mmol, 0.265 g) was added. The resulting solution was refluxed for 5 h. and then kept at room temperature. The pale-yellow crystals of **2** that separated out were filtered, washed with ether and dried over P_4O_{10} *in vacuo*.

[VO(DKN)(μ_2-O)]$_2$·2H_2O: Yield: 83%, m.p.: 182–184 °C. λ_m (DMF): 8 $ohm^{-1}\,cm^2\,mol^{-1}$. Elemental *Anal.* Calc. for [VO(DKN)(μ_2-O)]$_2$·2H_2O: C, 51.23; H, 3.69; N, 17.07. Found: C, 51.65; H, 3.23; N, 17.71%.

*2.3.3. Synthesis of [VO(QCB)(OMe)]·1.5H$_2$O (**3**)*

Complex **3** was prepared in similar manner as complex **2** by refluxing methanol solutions of HQCB (1 mmol, 0.303 g) and VO(acac)$_2$ (1 mmol, 0.265 g) for 5 h. A green crystalline precipitate was filtered, washed with ether and dried over P_4O_{10} *in vacuo*.

[VO(QCB)(OMe)]·1.5H_2O: Yield: 89%, m.p.: >300 °C. λ_m (DMF): 20 $ohm^{-1}\,cm^2\,mol^{-1}$. Elemental *Anal.* Calc. for [VO(QCB)(OMe)]·1.5H_2O: C, 54.14; H, 4.54; N, 10.52. Found: C, 53.73; H, 4.41; N, 10.63%.

*2.3.4. Synthesis of [VO(HQCN)(SO$_4$)]SO$_4$·4H$_2$O (**4**)*

Complex **4** was prepared in similar manner as complex **1** refluxing methanol solutions of HQCN (1 mmol, 0.303 g) and vanadyl

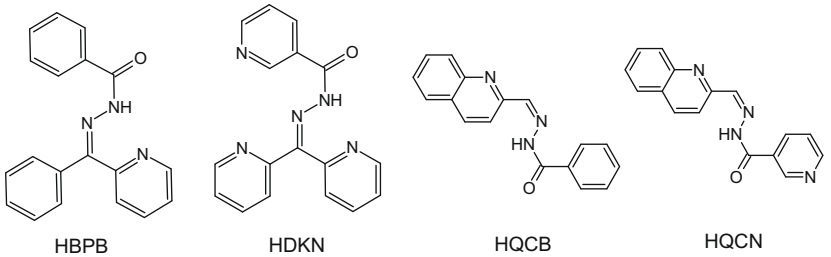

Fig. 1. Chemical structures of hydrazone ligands and their abbreviations.

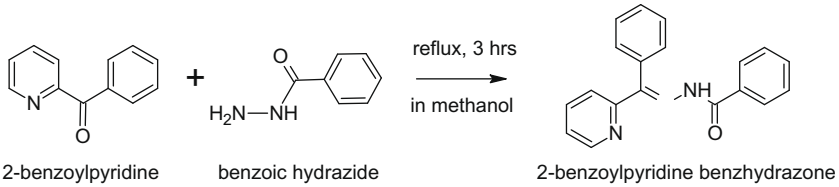

Scheme 1. Synthesis of 2-benzoylpyridine benzoyl hydrazone.

sulfate (1 mmol, 0.163 g) for 5 h. A green crystalline precipitate was filtered off, washed with ether and dried over P_4O_{10} *in vacuo*.

$[VO(HQCN)(SO_4)]SO_4{\cdot}4H_2O$: Yield: 63%, m.p.: 225–227 °C. λ_m (DMF): 62 $ohm^{-1}\,cm^2\,mol^{-1}$, Elemental *Anal.* Calc. for $[VO(HQCN)(SO_4)]SO_4{\cdot}4H_2O$: C, 37.58; H, 3.94; N, 10.96. Found: C, 37.44; H, 3.81; N, 10.72%.

2.4. Physical measurements

Elemental analyses of the ligands and the complexes were conducted on a Vario EL III CHNS analyzer at the SAIF, Kochi, India. The IR spectra were recorded on a Thermo Nicolet AVATAR 370 DTGS model FT-IR spectrophotometer as KBr pellets at SAIF, Kochi. Electronic spectra in CH_3CN solution were recorded on a Spectro UV–Vis Double Beam UVD-3500 spectrophotometer in the range 200–900 nm. The molar conductance of the complexes in DMF (10^{-3} M) solution was measured at 298 K with a Systronic model 303 direct-reading conductivity bridge. The EPR spectra of the complexes were recorded on a Varian E-112 spectrometer using TCNE as the standard at the SAIF, IIT, Bombay, India.

2.5. X-ray crystallography

Single crystal X-ray diffraction experiments for colourless HBPB and yellow **1** were performed on an Oxford CCD diffractometer with graphite monochromated Mo Kα radiation ($\lambda = 0.71073$ Å) [16]. The CrysAlis RED software was used for cell refinement and data reduction [16]. The structures were solved by direct-methods using SHELXS-97 [17] and each refinement was carried out by full-matrix least-squares on F^2 (SHELXL-97) [17] with anisotropic displacement parameters for non-hydrogen atoms and a weighting scheme of the form $w = 1/[\sigma^2(F_o^2) + (0 \cdot aP)^2 + bP]$, where $P = (F_o^2 + 2F_c^2)/3$). For HBPB, the nitrogen-bound hydrogen atom was located from a difference Fourier map and refined. The remaining hydrogen atoms in each model were placed in their calculated positions in the riding model approximation. As evident

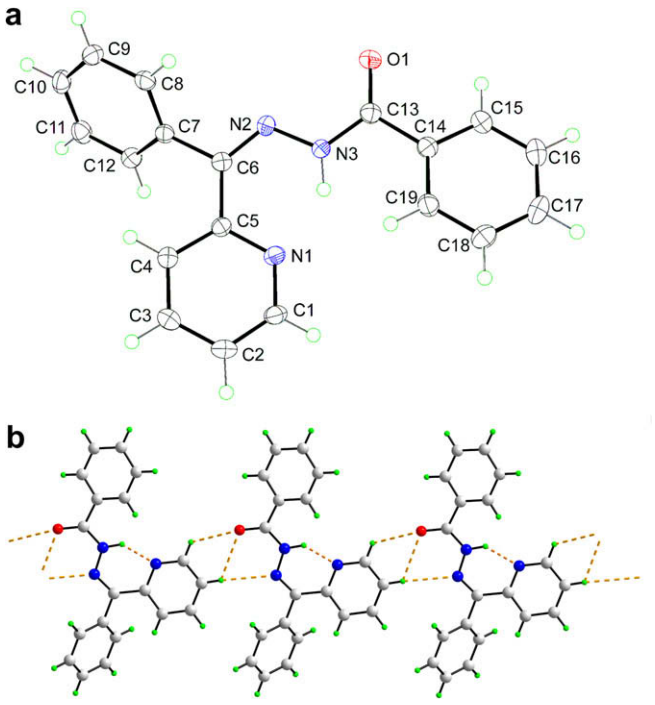

Fig. 2. (a) The molecular structure of HBPB along with the atom numbering scheme. (b) Supramolecular chain mediated by C–H···N and C–H···O contacts. These contacts and the intramolecular N–H···N hydrogen bonds are shown as orange dashed lines. Geometric details describing the intramolecular N3–H3n···N1 hydrogen bond in HBPB: H3n···N1 = 1.847(15) Å; N3···N1 = 2.6101(15) Å with angle at H3n = 139.6(14)°. Intermolecular interactions operating in the crystal structure of HBPB: C2–H2···$N2^i$ = 2.62 Å and C2···$N2^i$ = 3.5693(18) Å with angle at H2 = 174° for symmetry operation i: *x*, −1 + *y*, *z*. C1–H1···$O1^i$ = 2.63 Å and C1···$O1^i$ = 3.2565(18) Å with angle at H1 = 124°. C2–H2···$O1^i$ = 2.65 Å and C2···$O1^i$ = 3.2465(19) Å with angle at H2 = 121°. C11–H11···Cg(C14–C19)^{ii} = 2.86 Å; C11···Cg(C14–C19)^{ii} = 3.6300(17) Å with angle at H11 = 139° for ii: *x*, *y*, 1 + *z*.

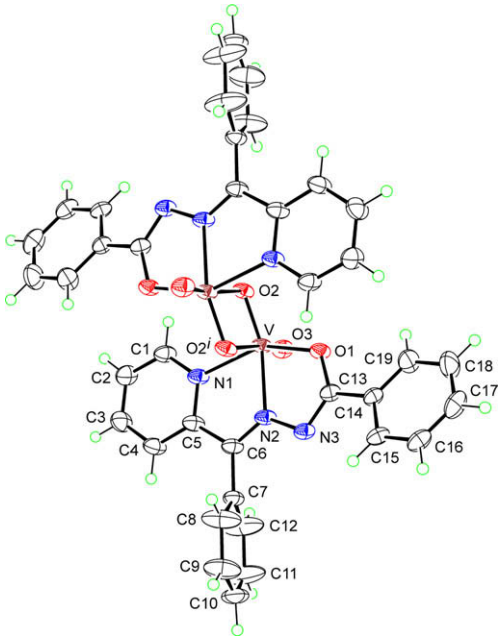

Fig. 3. The molecular structure of centrosymmetric $[VO(BPB)\mu_2\text{-}O)]_2$ (**1**) along with the atom numbering scheme. Symmetry operation i: −*x*, −*y*, 2 − *z*. Geometric details describing the closest intermolecular interactions operating in the crystal structure of **1**: C16–H16···$O2^i$ = 2.55 Å and C16···$O2^i$ = 3.286(3) Å with angle at H16 = 135° for symmetry operation i: ½ + *x*, ½ − *y*, −½ + *z*; C17–H17···$N3^{ii}$ = 2.56 Å and C17···$N3^{ii}$ = 3.447(4) Å with angle at H2 = 155° for symmetry operation ii: ½ − *x*, ½ + *y*, 1½ − *z*; π···π: Cg(N1,C1–C5)···Cg(N1,C1–C5)^{iii} = 3.6940(14) Å for iii: −1 − *x*, −*y*, 2 − *z*.

Table 1
Crystallographic and refinement details of complexes HBPB, $[VO(BPB)\mu_2\text{-}O)]_2$ (**1**) and $[VO(DKN)\mu_2\text{-}O)]_2{\cdot}½H_2O$ (**2**).

Compound	HBPB	**1**	**2**
Formula	$C_{19}H_{15}N_3O$	$C_{38}H_{28}N_6O_6V_2$	$C_{34}H_{25}N_{10}O_{6.5}V_2$
Formula weight	301.34	766.54	779.52
Crystal system	triclinic	monoclinic	triclinic
Space group	$P\bar{1}$	$P2_1/n$	$P\bar{1}$
a (Å)	8.0330(5)	9.9435(1)	8.0494(12)
b (Å)	8.6486(5)	9.9285(2)	9.750(2)
c (Å)	11.3168(8)	17.1187(2)	10.7678(19)
α (°)	89.329(5)	90	89.291(9)
β (°)	84.857(5)	90.464(1)	77.852(8)
γ (°)	72.332(5)	90	81.034(9)
V (Å^3)	746.03(8)	1689.97(4)	815.8(3)
Z	2	2	1
T (K)	150	150	98
D_c (g cm^{-3})	1.341	1.506	1.587
F(0 0 0)	316	784	397
μ(Mo Kα) (mm^{-1})	0.086	0.611	0.639
Measured data	6500	13 940	12 219
θ range (°)	3.0–25.0	3.1–25.0	2.8–26.5
Unique data	2625	2992	3325
Observed data ($I \geqslant 2.0\sigma(I)$)	2004	2476	3180
R, observed data; observed data	0.035; 0.079	0.036; 0.091	0.043; 0.103
a; *b* in weighting scheme	0.048; 0	0.045; 1.357	0.047; 0.923
R_w, observed data; all data	0.052; 0.084	0.047; 0.095	0.045; 0.104

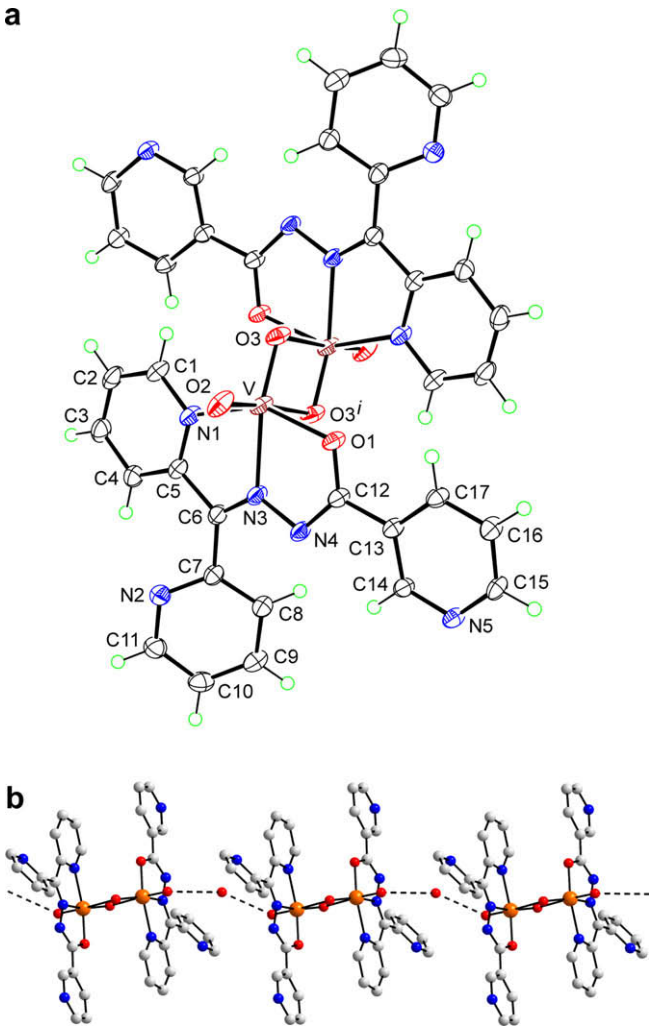

Fig. 4. (a) The molecular structure of centrosymmetric $[VO(DKN)\mu_2\text{-}O)]_2{\cdot}½H_2O$ (**2**) along with the atom numbering scheme. The solvent water molecule has been omitted for reasons of clarity. Symmetry operation i: $1-x, -y, 2-z$. (b) Supramolecular chain mediated by –O···H–O–H···O–hydrogen bonding (black dashed lines). Hydrogen atoms have been omitted for clarity. Geometric details describing the closest intermolecular interactions operating in the crystal structure of **2**: C9–H9···O2^{i} = 2.35 Å and C9···O2^{i} = 3.293(3) Å with angle at H9 = 172° for symmetry operation i: $x, 1+y, z$; C1–H1···N5^{ii} = 2.53 Å and C1···N5^{ii} = 3.331(3) Å with angle at H1 = 143° for symmetry operation ii: $1+x, -1+y, z$; π···π: Cg(N5,C13–C17)···Cg(N5,C13–C17)^{iii} = 3.6213(14) Å for iii: $-x, 1-y, 2-z$.

from Fig. 3, there is high thermal motion associated with the pendent C7–C12 aromatic ring. However, multiple sites were not discerned for this residue.

Intensity data for a pale-yellow prism of **2** were collected at 93 K on a Rigaku AFC12/Saturn724 CCD fitted with Mo Kα radiation. The data set was corrected for absorption based on multiple scans [18] and reduced using standard methods [19]. The structure was solved and refined using SHELXL-97 [17], as described above. A residual electron density peak, consistent with the presence of a disordered solvent water molecule was evident towards the end of the refinement. This was modelled as 0.25 of a water molecule proximate, over a centre of inversion (1.651(12) Å), to a centrosymmetric mate so that the crystal chosen for analysis is formulated as $[VO(DKN)(\mu_2\text{-}O)]_2{\cdot}½H_2O$; hydrogen atoms were not included for the water molecule.

Crystal data and refinement details are given in Table 1. Figs. 2–4, showing the atom labelling schemes were drawn with 50% displacement ellipsoids [20], and the remaining crystallographic figures were drawn with DIAMOND [21].

Table 2
Selected bond lengths (Å) and bond angles (°) for HBPB and $[VO(BPB)\mu_2\text{-}O)]_2$ (**1**).

	HBPB	**1**
C13–O1	1.2213(14)	1.300(3)
N2–N3	1.3682(15)	1.372(3)
N2–C6	1.2955(16)	1.291(3)
N3–C13	1.3610(16)	1.313(3)
O1–C13–N3	124.67(12)	124.3(2)
N3–N2–C6	117.38(10)	121.72(18)
N2–C6–C5	127.69(12)	112.6(2)
N2–C6–C7	114.35(10)	125.1(2)
N2–N3–C13	121.33(10)	107.09(17)
N3–C13–C14	112.84(10)	118.25(19)

3. Results and discussion

All the hydrazones discussed here are NNO donors and they can coordinate either in the keto form or in enolic form. All newly synthesized complexes are soluble in polar organic solvents such as chloroform, CH_3CN, DMF, DMSO, *etc.* Infrared spectral evidence supports the presence of coordination of the respective hydrazones through the enolate form in complexes **1**, **2** and **3**, while in complex **4**, the ligand coordinates in the keto form. The molar conductivity measurements in 10^{-3} M DMF solutions show non-electrolytic nature for complexes **1, 2** and **3** but complex **4** behaves as a 1:1 electrolyte [22]. Complexes **3** and **4** are EPR active due to the presence of an unpaired electron, while complexes **1** and **2** are EPR silent. The structures of complexes **1** and **2** have been confirmed by single crystal X-ray crystallography as has the structure of HBPB.

3.1. Crystal and molecular structure of HBPB

The colourless block-shaped crystals suitable for analysis were grown by slow evaporation from a methanolic solution of the HBPB. A perspective view of the compound showing the crystallographic numbering scheme is shown in Fig. 2a; selected geometric parameters are collected in Table 2. The central part of the molecule is essentially planar due to the presence of an intramolecular $N\text{–}H\cdots N_{pyridine}$ hydrogen bond. The maximum deviation from the least-squares plane calculated for the hydrazone moiety, i.e. C6–N2–N3–C13–O1, is 0.0189(12) Å for the N2 atom. The terminal aromatic rings are twisted out of this plane as seen in the values of the N2–C6–C7–C8 and N3–C13–C14–C15 torsion angles of −47.93(18) and 159.25(12)°, respectively. The dihedral angle formed between the terminal rings is 66.67(7)°. The C13–O1 bond distance of 1.2213(14) Å indicates the molecule exists in the keto form in the solid-state. The N2–C6 bond length is 1.2955(16) Å, with significant double-bond character, is comparable to those previously reported in analogous of hydrazone structures [23]. The above notwithstanding, the values of the N2–N3 and N3–C13 bond dis-

Table 3
Selected bond lengths (Å) and bond angles (°) for $[VO(BPB)\mu_2\text{-}O)]_2$ (**1**) and $[VO(DKN)\mu_2\text{-}O)]_2{\cdot}½H_2O$ (**2**).

V–O1	1.9563(16)	V–O1	1.9704(15)
V–O2	1.6589(16)	V–O3	1.6679(15)
V–O2^{i}	2.3475(17)	V–O3^{i}	2.3013(16)
V–O3	1.6092(18)	V–O2	1.6136(17)
V–N1	2.110(2)	V–N1	2.3013(16)
V–N2	2.1256(18)	V–N3	2.1298(18)
O2–V–O2^{i}	77.87(7)	O3–V–O3^{i}	77.91(7)
O2^{i}–V–O3	173.93(7)	O2–V–O3^{i}	175.08(8)
O1–V–N1	146.80(7)	O1–V–N1	146.97(7)
O1–V–N2	74.05(7)	O1–V–N3	74.72(6)
O2–V–N2	151.59(8)	O3–V–N3	152.32(7)
N1–V–N2	73.56(7)	N1–V–N3	72.92(7)
V–O2–V^{i}	102.13(7)	V–O3–V^{i}	102.09(7)

tances of 1.3682(15) and 1.3610(16) Å, respectively, indicate significant delocalization of π-electron density over the hydrazone portion of the molecule. The conformation about the N2–C6 bond is *Z*.

The principal feature of the crystal packing is the formation of a supramolecular chain mediated by cooperative C–H···N and C–H···O contacts; the formation of a chain mediated by amide ···O=C–N–H hydrogen bonds is precluded owing to the presence of the intramolecular N–H···$N_{pyridine}$ contact. The supramolecular chains, illustrated in Fig. 2b, are oriented along the *b*-direction and stack side by side with neighbouring chains to form layers approximately in the $(2\,0\,\bar{1})$ plane. The primary connections between layers are of the type C–H···π.

3.2. Crystal structures of $[VO(BPB)(\mu_2\text{-}O)]_2$ (**1**) and $[VO(DKN)\mu_2\text{-}O)]_2\cdot\frac{1}{2}H_2O$ (**2**)

Yellow diamond-shaped crystals of **1** were obtained by slow evaporation from a methanolic solution of **1**. The molecular structure and crystallographic numbering scheme is illustrated in Fig. 3 and relevant bond lengths and angles are listed in Tables 2 and 3 (vanadium coordination geometry). The binuclear complex is centrosymmetric, being disposed about a crystallographic centre of inversion. Each VO_2^+ is coordinated by the tridentate BPB anion via the pyridyl-N1, azomethine-N2 and enolic-O1 atoms [24]. The final position in the hexacoordinated geometry is completed by a bridging oxo-$O2^i$ atom. The coordination geometry is based on an octahedron with one triangular face defined by three oxygen atoms, i.e. O1, O2 and O3, and the other by the N1, N2 and $O2^i$ atoms; the major distortions from the ideal geometry are ascribed to the acute chelate angles, Table 3. The availability of the structural details for the HBPB molecule, see above, allows a comparison between the derived interatomic parameters.

From the data collected in Table 2, it is evident that there is significant elongation of the C13–O1 bond distance with a concomitant reduction in the N3–C13 bond upon coordination of BPB. These changes indicate BPB is functioning as an enolate ligand. The changes in bond distances are accompanied by some significant changes in the bond angles in BPB when the five-membered chelate rings are formed in the complex. Most notably, the N2–N3–C13 angle contracts by about 14° and the N2–C6–C7 angle widens by about 11°.

Selected bond distances and angles describing the vanadium atom geometry in **1** are summarised in Table 3. The V_2O_2 core is a parallelogram (1.66 × 2.35 Å) owing to the significant disparity of about 0.7 Å in the V–O2 and V–$O2^i$ bond distances; the terminal vanadyl–oxygen atoms, from symmetry, lie above and below this plane. The influence of the asymmetric bridging on the V=O bond distances is apparent so that the V–O2 distance, i.e. involving the bridging-O2 atom, of 1.6589(16) Å is longer than the V=O3 distance of 1.6092(18) (17) Å. The disparity in the bridging distances is partly ascribed to the observation that the longer V–$O2^i$ bond is *trans* to the terminal vanadyl–O3 atom. The V–N1 bond distance of 2.110(2) Å is marginally shorter than the V–N2 bond distance of 2.1256(18) Å. The intramolecular V···V bond distance is 3.1463(7) Å, which falls within the range of known V···V distances in doubly-bridged vanadium polynuclear systems [25,26].

To a first approximation, the molecular structure of the complex in $[VO(DKN)\mu_2\text{-}O)]_2\cdot\frac{1}{2}H_2O$ (**2**) resembles that just described, Fig. 4a and Table 3. In this case, the pyridine-N1 atom forms a significantly longer V–N1 bond, i.e. 2.3013(16) Å, compared with the V–N3 bond, i.e. 2.110(2) Å, formed by the azomethine-nitrogen atom. Significant differences in the V–O bond distances are also evident between **1** and **2**. Thus, in **2**, each of V–O1, V–O2 and V–O3 are longer but the bridging V–$O3^i$ distance is shorter. It is noted that with the exception of the elongation of the C5–C6 bond distance in **2** to 1.485(3) Å, compared with 1.460(3) Å in **1**, the bond distances defining the N1–C2–N2–C12–O1 backbones of the tridentate ligands in each of **1** and **2** are indistinguishable. In the absence of any obvious electronic influence exerted by the pendant pyridine residue in **2**, compared to phenyl in **1**, this reorganisation of electron density giving rise to disparate bond distances in the structures is ascribed to participation of solvent water in the (supramolecular) structure of **2**, see above.

The crystal structure of **1** is consolidated into a three-dimensional network by a C–H···O, C–H···N and π···π contacts. The intervention of solvent water in the crystal structure of **2**, Fig. 4b, leads to the formation of a supramolecular chain along the *c*-direction. While the solvent water molecule is only partially occupied and disordered across a centre of inversion, see Section 2, it forms significant alternating O···O interactions of 2.834(9) and 3.2923(9) Å with the vanadyl–O2 atom, Fig. 4b. Chains are consolidated into the crystal structure by a large number of C–H···O, C–H···N and π···π contacts.

3.3. Infrared spectra

The comparison of the main vibrational bands of the ligands with those of the complexes helps to establish their ligating behaviour to the metal centre. Selected IR bands of the complexes are represented in Table 4. The IR spectra of the ligands exhibit two bands at *ca.* 3089 and 1672 cm^{-1} due to the *ν*(NH) and *ν*(C=O)

Table 5
Electronic spectral assignments of the ligands and the complexes **1–4**.

Compound	UV–Vis λ_{max} (nm)
HBPB	322, 271, 233
(HDKN·0.5H_2O)	318, 269, 229
(HQCB·1.5H_2O)	326, 277, 240
(HQCN·1.5H_2O)	315, 279, 241
$[VO(BPB)\mu_2\text{-}O)]_2$ (**1**)	406, 282, 231
$[VO(DKN)\mu_2\text{-}O)]_2\cdot2H_2O$ (**2**)	402, 280, 233
$[VO(QCB)(OMe\cdot)]\cdot1.5H_2O$ (**3**)	856, 541, 422, 311, 277, 233
$[VO(HQCN)(SO_4)]SO_4\cdot4H_2O$ (**4**)	852, 409, 315, 275

Table 4
Infrared spectra (cm^{-1}) of hydrazones and their vanadium(IV/V) complexes.

Compound	*ν*(N–H)	*ν*(C=O)	*ν*(C=N)	*ν*(C=N)[a]	*ν*(C–O)	*ν*(V=O)	*ν*(V–O–V)
HBPB	2928	1689	1588				
(HDKN·0.5H_2O)	3063	1689	1571				
(HQCB·1.5H_2O)	3193	1655	1593				
(HQCN·1.5H_2O)	3173	1656	1591				
$[VO(BPB)\mu_2\text{-}O)]_2$ (**1**)			1509	1599	1368	946	853
$[VO(DKN)\mu_2\text{-}O)]_2\cdot2H_2O$ (**2**)			1509	1588	1373	945	853
$[VO(QCB)(OMe)]\cdot1.5H_2O$ (**3**)			1582	1593	1384	940	
$[VO(HQCN)(SO_4)]SO_4\cdot4H_2O$ (**4**)	3186	1655	1560			980	

[a] Newly formed C=N.

Table 6
EPR spectral assignments of oxovanadium(IV) complexes [VO(QCB)(OMe·)]·1.5H_2O (**3**) and [VO(HQCN)(SO_4)]SO_4·4H_2O (**4**) in the polycrystalline state at 298 K and in frozen DMF at 77 K.

Compound	Polycrystalline state (298 K)	DMF (77 K)	$A_{\|\|}$ [a]	$A_{\perp}$ [a]	β^2	α^2
3	1.941/1.947 ($g_{\|\|}/g_{\perp}$)		176.42	73.51		
4		1.928/1.978 ($g_{\|\|}/g_{\perp}$)	195.71	77.14	1.0335	0.756

[a] Expressed in units of cm^{-1} multiplied by a factor of 10^{-4}.

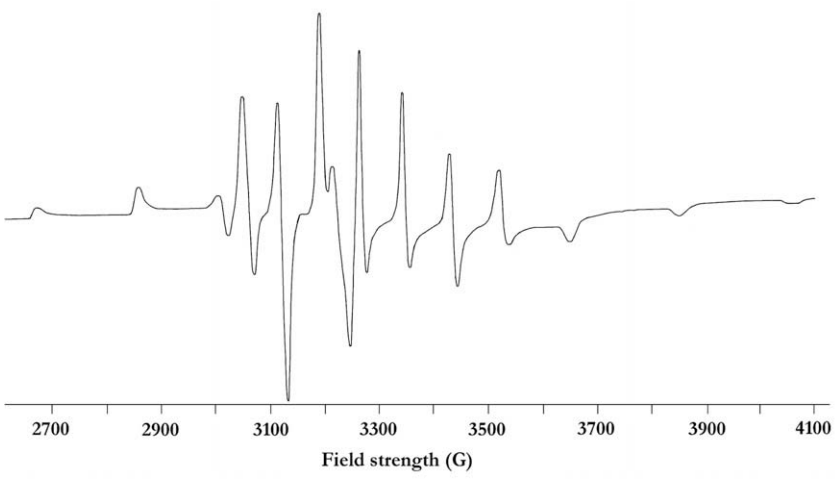

Fig. 5. EPR spectrum of [VO(HQCN)(SO_4)]SO_4·4H_2O (**4**) in DMF at 77 K.

stretches, respectively, and are indicative of their ketonic nature in the solid-state [27,28]. The existence of the ligand in the keto tautomer form was confirmed from the crystal structure determination (see above). These bands disappear on complexation in **1**–**3**. A new band appearing in the region 1360–1385 cm^{-1} is assigned to ν(C–O) indicating the involvement of the original carbonyl-oxygen in bonding as an enolate. However, in complex **4** no considerable shift is observed for the ν(C=O) and ν(NH) bands which implies that the ligand is coordinating in the keto form. Each of the aroylhydrazones under discussion display a strong and sharp band in the region 1570–1595 cm^{-1} ascribed to ν(C=N) of the azomethine group [29]. These bands undergo shifts to the lower wavenumbers upon complexation which suggest the coordination of the azomethine-nitrogen to vanadium. The presence of new bands in the region at *ca.* 1593 cm^{-1}, which may be due to the newly formed ν(C=N) bond except in complex **4**, confirms the coordination *via* azomethine-nitrogen. The out-of-plane bending modes of vibrations of the free ligands at 622 cm^{-1} are found to be shifted to higher energies in the spectra of complexes indicating the coordination *via* pyridine nitrogen [30]. Further, the intense band observed in the region 945-980 cm^{-1} in all the complexes corresponds to the terminal V=O stretching. In addition to this, the dimeric complexes **1** and **2** exhibit bands at *ca.* 853 cm^{-1} due to the V–O–V bridging vibrations [31]. In complex **4**, two sulfate ligands are present and accordingly in the IR spectrum, strong bands are observed at 1044 and 1170 cm^{-1}, due to ν_3, and 469 cm^{-1}, due to ν_2, which can be assigned to a bidentate bridging sulfato group; bands at 1126 and 606 cm^{-1} can be assigned to the presence of an ionic sulfato group [32].

3.4. Electronic spectra

The electronic absorption bands of the ligands and complexes are recorded in acetonitrile solution and all data are summarised in Table 5. The bands at *ca.* 320, 275 and 235 nm, attributed to the n–π^* and π–π^* transitions shifted upon complexation. For complexes **1** and **2**, high energy bands in the range 405 nm are assigned to the ligand to metal charge transfer (LMCT) transitions arising from phenolate oxygen of the ligand to an empty d orbital of the vanadium ion. These dioxo-vanadium(V) complexes have a d^0 configuration, and d–d bands are therefore not expected. For the oxovanadium complexes the bands at 415 nm are assigned to the charge transfer transitions arising due to the O(phenolate) → V^{4+} LMCT transitions. The two bands at 856 and 541 nm for **3** are due to the $d_{xy} \rightarrow d_{xz}$, d_{yz} and $d_{xy} \rightarrow d_{x^2-y^2}$ transitions, while in **4** only one d–d band at 852 nm is observed [33].

3.5. EPR spectra

The oxidation state of the central vanadium atom in the complexes was confirmed by the measurements of EPR spectroscopy. Complexes **3** and **4** are paramagnetic samples and EPR spectra were recorded in polycrystalline state at 298 K and in frozen DMF at 77 K. In polycrystalline state at 298 K, compound **3** is axial with $g_{\|}$ = 1.941 and $g_{\perp}$ = 1.947. In frozen DMF the complex **4** displayed well-resolved axial anisotropy characterized by two sets of eight lines which result from coupling of the electron spin to the spin of the ^{51}V nucleus ($I = {}^7/_2$). The EPR spectrum of complexes **3** in DMF at 77 K and **4** in polycrystalline state were not of good quality, probably due to poor glass formation in the case of **3**. Spectral parameters are collected in Table 6 and representative spectrum is displayed in Fig 5. The $g_{\|} < g_{\perp}$ and $A_{\|} > A_{\perp}$ relationship are characteristic of an axially compressed d^1_{xy} configuration [31]. The lower values for α^2 compared to β^2 indicate that in-plane σ-bonding is more covalent than in-plane π-bonding. For the dimeric vanadium complexes with VO_2^+ motif, vanadium is in +5 oxidation state and therefore EPR silent.

Acknowledgements

M.R.P. Kurup is thankful to CSIR, New Delhi, India [01(1963)/05/EMR-II] for financial assistance. S.R.S. thanks CSIR, New Delhi for the award of Senior Research Fellowship. The authors are thankful to the SAIF, Cochin University of Science and Technology, Kochi,

Kerala, India for elemental and IR analyses. We are thankful to IIT, Bombay, India for EPR analysis and National Single Crystal X-ray Diffraction Facility, IIT, Bombay, India for providing single crystal intensity data for HBPB and **1**.

Appendix A. Supplementary material

CCDC 686871, 686872 and 723096 contain the supplementary crystallographic data for HBPB, **1** and **2**. These data can be obtained free of charge from The Cambridge Crystallographic Data Centre via www.ccdc.cam.ac.uk/data_request/cif. Supplementary data associated with this article can be found, in the online version, at doi:10.1016/j.ica.2009.06.029.

References

[1] M.M. Heravi, L. Ranjbar, F. Derikvand, H.A. Oskooie, F.F. Bamoharram, J. Mol. Catal. A: Chem. 265 (2007) 186.
[2] R.C. Maurya, S. Rajput, J. Mol. Struct. 833 (2007) 133.
[3] Y. Adachi, J. Yoshida, Y. Kodera, A. Katoh, J. Takada, H. Sakurai, J. Med. Chem. 49 (2006) 3251.
[4] K.H. Thompson, Biofactors 10 (2008) 43.
[5] M.R. Maurya, S. Agarwal, C. Bader, D. Rehder, Eur. J. Inorg. Chem. (2005) 147.
[6] M.R. Maurya, A. Arya, A. Kumar, J.C. Pessoa, Dalton Trans. (2009) 2185.
[7] S.S. Amin, K. Cryer, B. Zhang, S.K. Dutta, S.S. Eaton, O.P. Anderson, S.S. Miller, B.A. Reul, S.M. Brichard, D.C. Crans, Inorg. Chem. 39 (2000) 406.
[8] F. Montilla, D. del Rio, A. Pastor, A. Galindo, Organometallics 25 (2006) 4996.
[9] K. Nomura, Y. Onishi, M. Fujiki, J. Yamada, Organometallics 27 (2008) 3818.
[10] P. Noblía, M. Vieites, B.S. Parajon-Costa, E.J. Baran, H. Cerecetto, P. Draper, M. González, O.E. Piro, E.E. Castellano, A. Azqueta, A.L. de Ceráin, A. Monge-Vega, D. Gambino, J. Inorg. Biochem. 99 (2005) 443.
[11] D.C. Crans, Y. Yang, T. Jakusch, T. Kiss, J. Inorg. Chem. 39 (2000) 4409.
[12] S. Rayati, A. Wojtczak, A. Kozakiewicz, Inorg. Chim. Acta 361 (2008) 1530.
[13] Z.-P. Li, Y.-H. Xing, Y.-Z. Cao, X.-Q. Zeng, M.-F. Ge, S.-Y. Niu, Polyhedron 28 (2009) 865.
[14] L. Leelavathy, S. Anbu, M. Kandaswamy, N. Karthikeyan, N. Mohan, Polyhedron 28 (2009) 903.
[15] P.V. Bernhardt, G.J. Wilson, P.C. Sharpe, D.S. Kalinowski, D.R. Richardson, J. Biol. Inorg. Chem. 13 (2008) 107.
[16] CrysAlis CCD and CrysAlis RED Versions 1.171.29.2 (CrysAlis 171. NET), Oxford Diffraction Ltd., Abingdon, Oxfordshire, England, 2006.
[17] G.M. Sheldrick, Acta Crystallogr. A 64 (2008) 211.
[18] T. Higashi, ABSCOR, Rigaku Corporation, Tokyo, Japan, 1995.
[19] CrystalClear User Manual, Rigaku/MSC Inc., Rigaku Corporation, The Woodlands, TX, 2005.
[20] L.J. Farrugia, J. Appl. Crystallogr. 30 (1997) 565.
[21] K. Brandenburg, DIAMOND, Visual Crystal Structure Information System, Version 3.1, CRYSTAL IMPACT, Postfach 1251, D-53002 Bonn, Germany, 2006.
[22] W.J. Geary, Coord. Chem. Rev. 7 (1971) 81.
[23] B.N. Bessy Raj, M.R.P. Kurup, Spectrochim. Acta Part A 66 (2007) 898.
[24] E.B. Seena, N. Mathew, M. Kuriakose, M.R.P. Kurup, Polyhedron 27 (2008) 455.
[25] B. Mondal, M.G.B. Drew, R. Banerjee, T. Ghosh, Polyhedron 27 (2008) 3197.
[26] A. Sreekanth, H.-K. Fun, R.P. John, M.R.P. Kurup, S. Chantraproma, Acta Crystallogr. E 62 (2006) 1919.
[27] A. Ray, S. Banerjee, S. Sen, R.J. Butcher, G.M. Rosair, M.T. Garland, S. Mitra, Struct. Chem. 19 (2008) 209.
[28] A.A.R. Despaigne, J.G. Da Sila, A.C.M. do Carmo, O.E. Piro, E.E. Castellano, H. Beraldo, Inorg. Chim. Acta 362 (2009) 2117.
[29] S. Naskar, D. Mishra, R.J. Butcher, S.K. Chattopadhyay, Polyhedron 26 (2007) 3703.
[30] P.F. Raphael, E. Manoj, M.R.P. Kurup, Polyhedron 26 (2007) 5088.
[31] N.A. Mangalam, M.R.P. Kurup, Spectrochim. Acta Part A 71 (2009) 2040.
[32] K. Nakamoto, Infrared and Raman Spectra of Inorganic and Coordination Compounds, 5th ed., Wiley, New York, 1997.
[33] T. Ghosh, S. Bhattacharya, A. Das, G. Mukherjee, M.G.B. Drew, Inorg. Chim. Acta 358 (2005) 989.